PCCP

Binary Cooperative NiCo2O4 on the Nickel Foams with Quasi-two-dimensional precursors: A Bridge between 'Supercapacitor' and 'Battery' in Electrochemical Energy Storage

Journal:	*Physical Chemistry Chemical Physics*
Manuscript ID:	CP-ART-11-2014-005228.R1
Article Type:	Paper
Date Submitted by the Author:	07-Dec-2014

Complete List of Authors:	Peng, Tao; Harbin Engineering University, School of Material Science and Chemical Engineering Qian, Zhongyu; Harbin Engineering University, School of Material Science and Chemical Engineering Wang, Jun; Harbin Engineering University, School of Material Science and Chemical Engineering Qu, Liangti; Beijing Institute of Technology, Key Laboratory of Cluster Science Wang, Peng; Chinese Academy of Sciences, State Key Laboratory of Polymer Physics and Chemistry, Changchun Institute of Applied Chemistry

Journal Name

RSCPublishing

ARTICLE

Binary Cooperative $NiCo_2O_4$ on the Nickel Foams with Quasi-two-dimensional precursors: A Bridge between 'Supercapacitor' and 'Battery' in Electrochemical Energy Storage

Cite this: DOI: 10.1039/x0xx00000x

Received ooth January 2012,
Accepted ooth January 2012

DOI: 10.1039/x0xx00000x

www.rsc.org/

Tao Peng,[a] Zhongyu Qian,[a] Jun Wang,*[,a] Liangti Qu[b] and Peng Wang[c]

Some inorganic quasi-two-dimensional nanomaterials, such as cobalt/nickel hydroxides, are kinetically facile for a capacitive charge storage process. However, high performance capacitive charge storage needs a balance the ionic and electronic transporting, to build up an integrated architecture on substrates step by step and utilize the interface better is still a key challenge. As the interfacial assembly has conflicted with our goals for high-performance capacitive charge storage process, we identify theoretically and experimentally binary cooperative nanoscale interfacial materials to solve the problem. Co-Ni-hydroxide precursors were prepared by hybrid quasi-two-dimensional nanosheets and hetero-oriented nanocrystallines walls. Followed by a dip-dry and annealing, $NiCo_2O_4$ could adhere to the nickel foams robustly with a solution-based surface treatment. Moreover, an unusual phenomenon in the electrochemical test inspired us to establish a bridge between 'supercapacitor' and 'battery'. The bridged gap highlights a new design idea for high-performance energy storage.

1. Introduction

Graphene's success has promoted processes and opportunities in few-layered or quasi-two-dimensional nanomaterials for their distinctive properties, such as ultrathinness, flexibility and charge-bearing in a plane.[1] Recent research has also focused on the design of ultrathin nanosheets including metal oxide (hydroxide) and metal disulfides.[2-3] Nevertheless, it seems that quasi-two-dimensional nanomaterials have successed in the fabrication rather than in the interfacial assembly. Liquid exfoliation of layered nanomaterials is an important advance,[4] while, high-concentration aqueous dispersion is still a demanding work[5] Recently, some bottom-up strategies for intercalation-exfoliation have deserved specific attention, such as $Co(OH)_2$,[6] $Ni(OH)_2$,[7] V_2O_5,[8] VS_2.[9] These inspire us that quasi-two-dimensional nanomaterials could be prepared directly, rather than in an exfoliation way.

Considering that some inorganic quasi-two-dimensional nanomaterials, such as cobalt/nickel hydroxides, are kinetically facile for a capacitive charge storage process.[10-12] Layered assembly with graphene-based nanomateirals has been intensively investigated by flocculation or layer-by-layer to offer a reinforcement of each other.[13-15] For capacitive charge storage, high power also needs a good electrical conductivity.[16] Therefore, interface design should balance the ionic and electronic transporting. Controllable microstructures grown on substrates have achieved notable success with a robust interface and enhanced electronic transporting.[17] Although quasi-two-dimensional nanomaterials are highly active for interfacial assembly, to build up an integrated architecture on substrates step by step and utilize the interface better is still a key challenge. The challenge has centered around the following: (1) Before an interfacial assembly, quasi-two-dimensional nanomaterials should be dispersed with high-concentration. (2) Moderate interaction induces the interfacial assembly to construct optimized space. (3) After the interfacial assembly, quasi-two-dimensional nanomaterials should adhere to the substrate robustly, the interface also needs a stability in an electrochemical process.

As a proof-of-concept demonstration, we present a simple and flexible solution-based strategy, as illustrated in Sch.1. First, binary cooperative Co-Ni-hydroxide precursors were prepared by hybrid quasi-two-dimensional nanosheets (QTD) and hetero-oriented nanocrystallines walls (HNW). Next, three-dimensional porous nickel foams with cobalt-nickel-hydroxide coating were prepared by a solution-based surface treatment. Consequently, followed by a dip-dry and annealing, $NiCo_2O_4$ could adhere the nickel foams robustly. Thus , binary

cooperative $NiCo_2O_4$ on the nickel foams construct a bridge between multiple redox pseudocapacitor and nanosized battery in electrochemical energy storage. Different from a transition from 'supercapacitor' to 'battery', they could exhibit adjustable hybrid behaviors between 'supercapacitor' and 'battery'

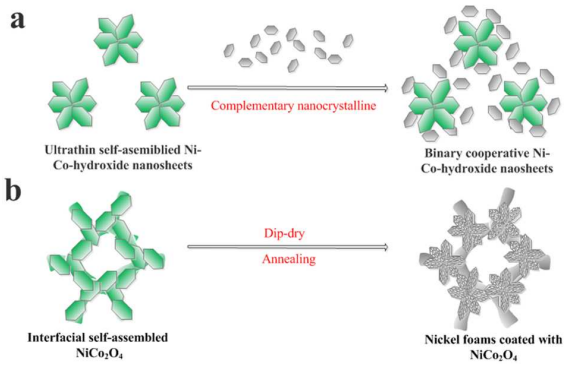

Sch.1 Schematic illustration of the binary cooperative $NiCo_2O_4$ on the nickel foams. (a) Preparation of binary cooperative Co-Ni-hydroxide precursors; (b) Interfacial assembly with treated nickel foams.

2. Experimental

2.1 Surface Treatment of the Nickel Foams

All the chemicals were directly used after purchase without further purification. The surface treatment was prepared by a published method reported with a little modification.[18] Nickel foams (50×25×1 mm^3, PPI: 110) were rolled to a thickness of 0.5 mm before use. The nickel foams were immersed in a 3 M HCl solution for 15 min and soaked in a 0.02 M $NiCl_2$ before they were used. $Ni(NO_3)_2$ (1.2 mmol) and $Co(NO_3)_2$ (2.4 mmol) were dispersed in 48 mL deionized water, hexamethylenetetramine (HMT, 7.2 mmol) in 24 ml ethanol was added, the mixed solution was then transferred to a 100 mL sealed bottle. A piece of nickel foams was dipped into the dispersion, and the bottle was heated at 90 °C in a water bath for 2 h.

2.2 Interfacial Assembly of $NiCo_2O_4$ on the Nickel Foams

$Ni(NO_3)_2$ (20 mmol) and $Co(NO_3)_2$ (40 mmol) were dispersed in 800 mL deionized water, hexamethylenetetramine (120 mmol) in 400 ml ethanol was added, and the mixed solution was heated with stirring at 90 °C in a water bath for 2 h. The product was isolated by three cycles of centrifugation/ washing/dispersion with deionized water, the concentrated suspension could be prepared by dispersing the product in 120 mL deionized water. The suspensions above (0, 10, 20, 40 mL) were diluted with deionized water to 50 mL, and $NiCl_2$ (6.7 mmol) and $CoCl_2$ (13.3 mmol) were dispersed. 1.9 g of NaOH in 50 ml water-ethanol mixed solvent (1/4, V/V) was slowly added. The suspensions were marked as QTD0, QTD10, QTD20, QTD40, respectively. The mixtures were digested for 0.5 h with stirring.

The nickel foam with the solution-based surface treatment was dipped into the dispersion and immediately removed. After drying in an electrical oven at 90 °C for 15 min, the dip-dry process was repeated one time to increase the loading on the nickel foam. The nickel foam was rinsed with deionized water and ethanol to remove residual ions, followed by annealed at 320 °C for 2 h.

2.3 Characterization

The crystallographic structures of the materials were determined by a powder XRD system (Rigaku TTR-III) equipped with Cu Kα radiation (λ = 0.15406 nm); The microstructure of the samples was investigated by SEM-EDS (JEOL JSM-6480A microscope), and TEM (Philips CM 200 FEG 200 kV).

2.4 Electrochemical Measurements

$NiCo_2O_4$/nickel foams were used as working electrodes (1 cm × 1.5 cm, projected area of 1 cm × 1 cm). Electrochemical measurement was carried out on a CHI 760B electrochemistry workstation. Measurements were studied on a three-electrode system (consisting of a working electrode, a platinum foil (1 cm × 1 cm) counter electrode, a saturated calomel electrode (SCE) reference electrode, and 2 M KOH aqueous solution as electrolyte).

2.5 Calculations

For cyclic volammograms, capacitance and specific capacitance (F cm^{-2}) are calculated in the three-electrode configuration using the formula:

$$C=I/v \quad (1)$$

$$Cs=\int IdV/(2vA\Delta V) \quad (2)$$

where I (A) is the response current, ν is the scan rate (V/s), ΔV is the applied potential region (V), A refers to the area (cm^2) of the electrode, and the integration is the area of the cyclic volammograms.

For electrochemical impedance spectra (EIS), specific capacitance (F cm^{-2}) is calculated in the three-electrode configuration using the formula:

$$C=-Z''/(2\pi f|Z|^2) \quad (3)$$

where Z'', |Z| is the real imaginary part and the model of the impedance, respectively. f is the frequency.

For galvanostatic charge-discharge curves, capacitance, specific capacitance (F cm^{-2} or F g^{-1}), equivalent series resistance (ESR, Ω), specific factor are calculated in the three-electrode configuration using the formula:

$$Cs=It/(\Delta VA) \quad (4)$$

$$Cm=It/(\Delta Vm) \quad (5)$$

$$R=Vdrop/(2I) \quad (6)$$

$$k=\int VdQ/EQ=\int Vdt/\Delta Vt \quad (7)$$

where I (A) is the discharge current, t is the discharge time (s), ΔV is the applied potential region (V), A refers to the area (cm^2) of the electrode, m (g) is the mass of the active materials, and Vdrop (V) is estimated from the voltage drop at the beginning of the discharge curve.

3. Results and discussion

Liquid exfoliation has succeed in cobalt-nickel-hydroxide nanosheets.[19] From a bottom-up thought, QTD could be prepared if the growth along the interlayers was inhibited. Therefore, an adjusted solution-based hydrolysis of HMT promotes the formation of QTD.[20] As shown on Fig. 1.a, layered QTD are piled up to a sheet with folded flower-like space. For the complementary nanomaterials, slowly added NaOH could benefits a high supersaturation and burst nucleation also could limits the growth of particles.[21] As shown on Fig. 1.b, hexagonal nanosheets are connected by irregular clusters or piles cluttered with minute folded nanosheets. Mesoscale self-assembled HNW could be transformed from the nanocale building blocks. Moreover, the characteristic (003) and (006) reflections confirm the hydrotalcite-like phase in XRD, the differences in crystallinity are in accordance with the size distributions for QTD and HNW. (Fig. S1.a)

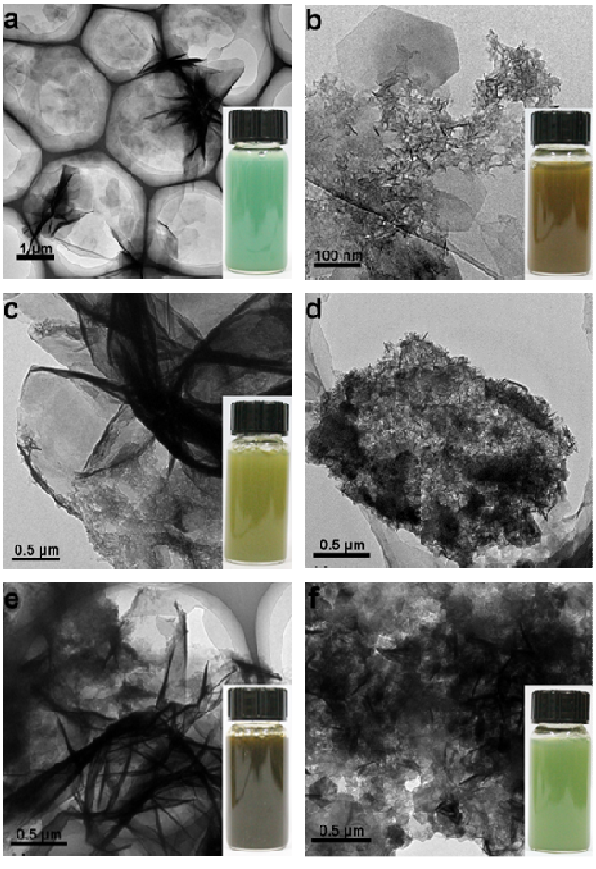

Fig. 1 TEM images of the suspensions with different content. (a:QTD; b:QTD0;c,d: QTD10; e: QTD20;f:QTD40). The insets in panels show bottles of the suspensions.

In the sight of the crystal growth mechanism for building binary cooperative cobalt-nickel-hydroxde, 'self-assembly' and 'oriented attachment' describes the spontaneous self-organization and joining of adjacent particles at the interface.[22] Mesoscale transformations of HNW into superstructures could be distinguished in TEM images.[23] (Fig. 1.c-f) Core QTD could act as backbones to guide the shell nanocale building blocks. Small QTD is more easily covered than folded flower-like, (Fig. 1.c,d) and the edges of QTD could be etched, (Fig. 1.e) or even ingested by the nanocale building blocks. (Fig. 1.f) Ions in the suspensions are generally considered to adsorb at edges to benefit the well dispersion of nanoscale building blocks, ion-by-ion attachment would also promote the unit replication when the kinetically metastable species are disturbed.[22-23] In fact, QTD could hardly be atom-thick, and perhaps the mesocrystals are more like gels than sols. Nevertheless, the property benefits a robust interface for the interfacial assembly.

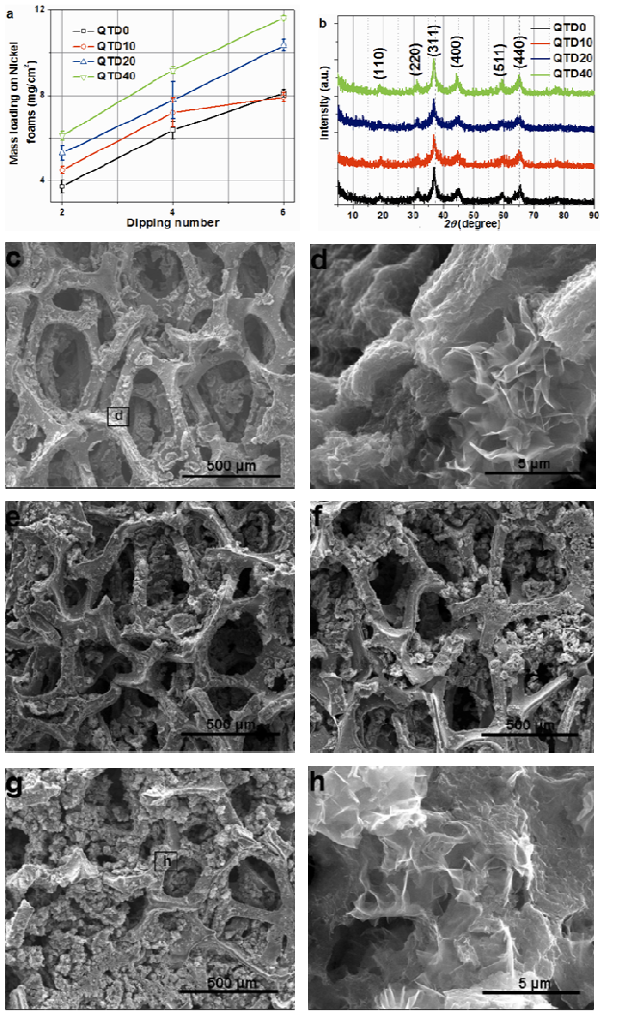

Fig. 2 Characterizations of the self-assemblied binary cooperative $NiCo_2O_4$. (a) Mass loading of the nickel foam with the surface treatment versus dipping number with different QTD contents. (b) XRD of the $NiCo_2O_4$ scratched from the self-assemblied nickel foams. (c-h) SEM images of the NCH/rGO/nickel foams. (c,d:QTD0; e:QTD10; f: QTD20; g,h: QTD40).

To promote the interfacial assembly process, three-dimensional porous nickel foams were selected as the conductive scaffolds with a simple solution method. 3D porous precursors could grow on the scaffolds. (Fig. S1.b) For a solution-based process, evaporation-induced is highly flexible for interpenetrating solid with gas. Fig. 2a shows the characteristic of the variation of the mass with the dipping number. Added QTD benefit a large mass loading. The mass loading increases uniformly with the dipping number except QTD10. It seems that the variation of QTD10 will approach a point of saturation. Despite different suspensions in QTD contents, similar spinel $NiCo_2O_4$ are prepared after annealed. (Fig. 2b)

A 'hit and stick' behavior could also describe the forming of fractal nanoparticle networks in the solvent-evaporation-induced interfacial self-assembly together with diffusion-limited cluster aggregation.[24] HNW could stand by the skeletons of the nickel foams densely. (Fig. 2.c,d) As QTD added, the aggregations could stand out the skeletons and cover the pores. (Fig. 2.e-h) QTD tends to roll to folded self-assembled clusters. (Fig. S2.a-d) The interval space formed between neighboring sheets makes easy diffusion of ion-transporting region. Moreover, the microstructure of aggregations may transform from NHW-based to QTD-based as QTD increased. Maybe the interfacial assembly is rough and random, while, the binary complementary nanomaterials guarantee a nanoscale spatial precision. NHW provide a robust adhesion, QTD promotes an optimal physical space.

To explore the electrochemical performances of the binary cooperative $NiCo_2O_4$ on the nickel foams, cyclic voltammetry was tested by a three-electrode system. (Fig. 3.a) Both of the anodic and the cathodic peaks shift towards the boundaries of the potential window as QTD increases, and the curves deviate from a central symmetric sharp. QTD40 exhibits a larger peak current than others. The peak current (I) is a function of the scan rate (v) and can generally be expressed as[25-26] :

$$I=av^b \qquad (8)$$

where a and b are the adjustable values. With the adjustable values, surface-controlled (b=1) and diffusion-controlled (b=0.5) could be distinguished (Figure 3b). For QTD10, b value range from 0.75 to 0.50 at the scan rates between 5 and 50 mVs^{-1}, indicating that the capacitive contribution from electric double layer. However, the b value of QTD40 mainly lower than 0.5 with the increase of scan rate from 20 to 50 mVs^{-1}, revealing that t charge storage was dominated by ohmic contributions and diffusion limitations.

Because the peaks shift differently in the cyclic voltammetry, the electrodes are also evaluated by the charging/discharging measurement at different potential windows. (Fig. 3.c) For specific capacitance, (Fig. 3.d) QTD40 is the top value for both the electroactive materials and the electrodes, (Fig. S3.a) and QTD0 lies in the bottom. QTD10 and QTD20 have a similar area specific capacitance, QTD10 could be better when the mass loading is considered. One feature of specific capacitance versus discharge current is that sometimes the specific capacitance could increase as the discharge current increase. It could be attributed to the decreased charge capacitance and the increased coulombic efficiency. (Fig. S3.b,c) EIS also has a similar result with b-value versus scan rate. (Fig. 3.e,f)

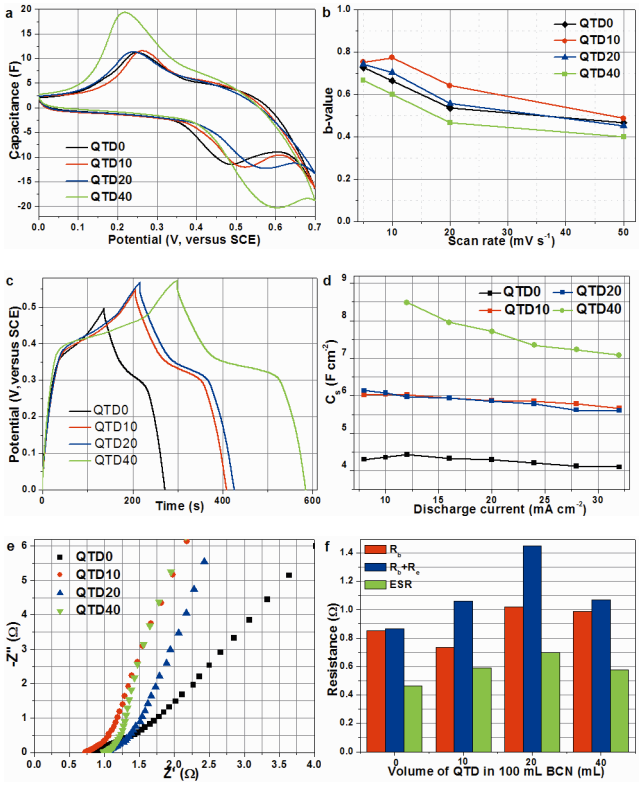

Fig. 3 Electrochemical characterizations of binary cooperative $NiCo_2O_4$ on the nickel foams. (a) Cyclic volammograms for different QTD contents at a scan rate of 5 mV s^{-1}. (b) b-value determination of the peak cathodic currents from 5 to 50 mV s^{-1}. (c) Charge and discharge curves at a current density of 16 mA cm^{-2}. (d) Specific capacitance (F cm^{-2}) versus current density. (e) EIS at 0 V. (f) Resistance (R_e, interface resistance between electrolyte and electrode; R_e, chargetransfer resistance, both calculated by EIS) calculated by EIS and discharge curves.

It could be inferred that the electrochemical process has a transition from 'supercapacitor' to 'battery' behavior,[27] which responds to the transition of the electroactive materials from NHW-based to QTD-based as QTD increased. However, differences in resistance by EIS and discharge curves imply that some issues during the process have not been adequately tackled. (Fig. 4.f, S3.d) Therefore, the potential values about the redox peaks are calculated by cyclic volammograms to discuss the process further. (Fig. 4.a,b) Although the peak separation responds to a thermodynamic irreversibility, the half-maximum line widths are almost independent of the scan rate. Surprisingly, after the relationship between cathodic peak and scan rate has been established, (Fig. 4c) QTD40 is more likely kinetically reversible with the linear fitting.[27] (Table S1) Moreover, the capacitance calculated by EIS at 10 mHz confirms bound redox processes as QTD added, the top is anchored at 0.5 V.

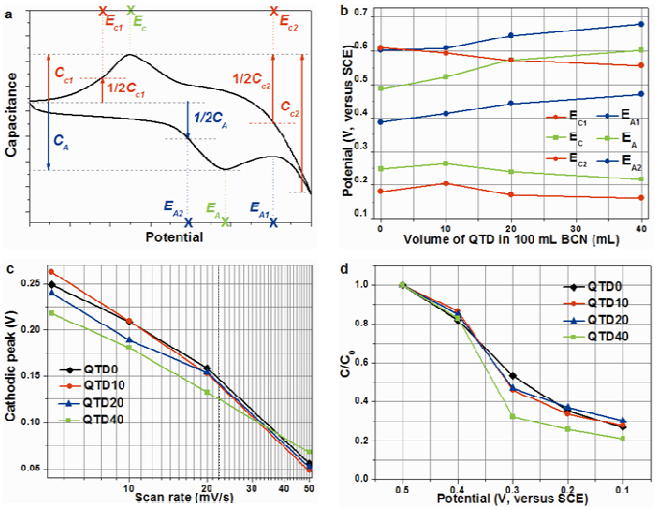

Fig. 4 Thermodynamic comparison of battery and supercapacitor behavior. (a) Schematic illustration of E value calculated by cyclic volammograms. (b) E value at at a scan rate of 5 mV s^{-1}. (c) The variation of the cathodic peak potential with the scan rate. (d) The capacitance calculated by EIS at 10 mHz.

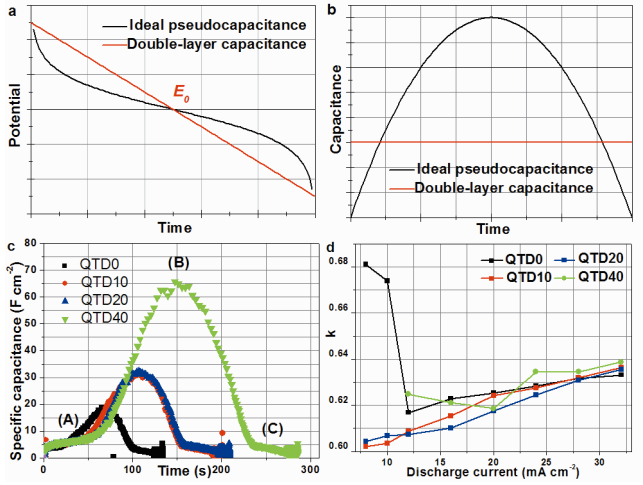

Fig. 5 Kinetic comparison of battery and supercapacitor behavior. (a) Schematic illustration of discharge curves for ideal pseudo- and double-layer capacitance. (b) Schematic illustration of capacitance in a discharge process. (c) Specific capacitance at 16 mA cm^{-2} during the discharge process. (d) K versus current density.

The results are often not analogous to others, and values in different orders with different tests imply that the transition is not the single. The strange features indicate that the binary cooperative $NiCo_2O_4$ on the nickel foams may exhibit an adjustable hybrid behavior of 'supercapacitor' and 'battery', rather than a transition from 'supercapacitor' to 'battery'. To verify our guess, we start from the origin of supercapacitor. According to Conway, supercapacitor could be divided into double-layer capacitor and pseudocapacitance.[27-29] For double-layer capacitor, the discharge curve could be generally expressed as:

$$U = E - \frac{It}{C} \qquad (9)$$

for pseudocapacitance, U is a function between the fractional extent of charge storage, X, and the conditional potential, E_0 [30]:

$$U = E_0 + \frac{RT}{nF} \ln \frac{X}{1-X} \qquad (10)$$

the discharge curve could be generally expressed as:

$$U = E_0 - \frac{RT}{nF} \ln \frac{t_0 - t}{t} \qquad (11)$$

where E is the initial potential, I is the discharge current, t is the discharge time (s), C is the constant capacitance, U is the potential that corresponds to t, R is the ideal gas constant, T is the thermodynamic temperature, F is Faraday's constant, n is the number of electrons involved in the reaction, and t_0 is the equivalent time for discharge fully. Then the discharge curves could be compared with our result. (Fig. 5.a) However, the discharge curves always deviate from an ideal sharp, the relationship between capacitance and time could be established to overcome the problem. Specific capacitance could be generally expressed as:

$$C = \left| \frac{I}{dU/dt} \right| \qquad (12)$$

for ideal pseudocapacitance, the relationship could be generally expressed as:

$$C = \frac{nFI}{RT} \frac{t}{t_0} \left(1 - \frac{t}{t_0}\right) \qquad (13)$$

Compared with Fig. 5.b, maybe it's better to say our discharge behavior contains three overlapped processes. (Fig. 5.c) Based on recent researches, the process should be expressed as [31-33]:

$$CoO_2 + H_2O + e^- \xrightarrow{A} CoOOH + 0H^- \qquad (A)$$

$$CoOOH + NiOOH + e^- \xrightarrow{B} H_2O + 0H^- + NiCo_2O_4 \qquad (B)$$

$$E_s // OH^- + e^- \xrightarrow{C} E_s + 0H^- \qquad (C)$$

(C) is expected to represent a double-layer process, but it is highly pesudocapacitive. From a battery view, the discharge curve of a nanosized battery material with a solid-solution phase transition will be highly similar to our results.[34-35] Specific factor is calculated to discover a feasible link between the them. All k values are between an ideal battery (k=1) and an ideal supercapacitor (k=0.5). The results indicate that all the electrodes have similar hybrid processes of "supercapacitor" and "battery".

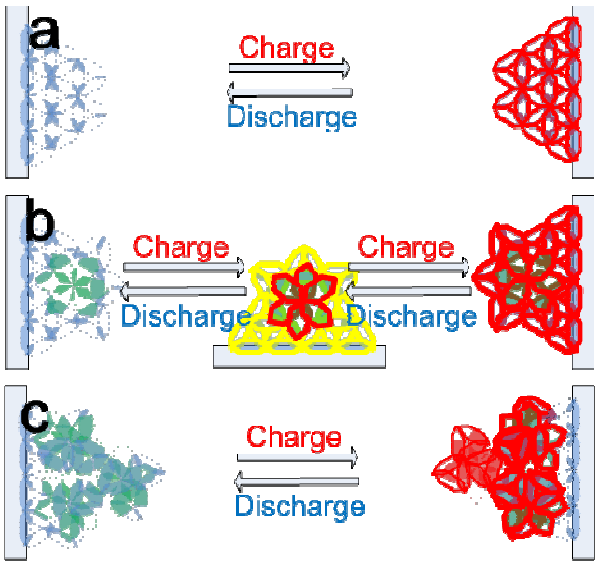

Sch.2 Schematic illustration of the binary cooperative $NiCo_2O_4$ on the nickel foams in an electrochemical process. (a) Ideal pseudocapacitance, charge and discharge occur near the surface of the electroactive materials; (b) Multi-stage pseudocapacitance, charge and discharge could occur with multiple redox processes, the same electrode could be in more than one state in the different regions; (c) Nanosized battery materials, charge and discharge could occur in individual particles one-by-one with coexisting phases, not all of the particles simultaneously, due to the interface effects.

To comprehend the hybrid process better, schematic illustrations at different conditions are used. For an ideal pseudocapacitance, charge and discharge occur near the surface of the electroactive materials, which promotes a kinetically facile and reversible in themodynamics[27-29.] (Sch. 2.a) When the electrochemical process involves multiple redox reactions, the same electrode could be in multiple charged states in the different regions. (Sch. 2.b) For a nanosized battery materials, heterogeneity and interfacial effect often lead to multiple charged states and thermodynamic hysteresis.[35-36] (Sch. 2.c) Binary cooperative $NiCo_2O_4$ on the nickel foams are between a continuous network and a non-monotone pariticle-by-particle structure. It can be inferred that highly capacitive regions and highly battery-like regions exist at once. A high specific capacitance for an electroactive material is generally associated with a diffusion-controlled process, which also suffers a low power with a transition from "pseudocapacitor" to "battery" behavior.[27] Nevertheless, ESR in discharge indicates that binary cooperative $NiCo_2O_4$ hardly suffers from a low power.

Thus, binary cooperative $NiCo_2O_4$ on the nickel foams construct a bridge between multiple redox pseudocapacitor and nanosized battery in electrochemical energy storage. Different from a transition from “supercapacitor” to “battery”, they could exhibit adjustable hybrid behaviors between “supercapacitor” and “battery”. As described by Jiang, binary cooperative interfacial materials could retain an opposite perforamace rather than an enhanced performance at the cost of the other.[17] The hybrid behavior could be cooperative and complementary. It inspires us some new design ideas as the following: (1) An electrode could combine “supercapacitor” with “battery” rather than two asymmetric electrodes. (2) Spinel $NiCo_2O_4$ is a better electronic conductor than insertion battery materials.[37-38] It may be attractive to design an aqueous high-power battery. (3) It is possible that a pseudocapacitive behavior could be received by binary cooperative battery and double-layer materials.

4. Conclusions

From a bottom-up thought, an adjusted solution-based hydrolysis of HMT promotes the production of QTD. For the complementary nanomaterials, slowly added NaOH benefits a high supersaturation, burst nucleation could limit the growth of particles. To promote the interfacial assembly process, three-dimensional porous nickel foams were selected as the conductive scaffolds with a simple solution method. Followed by a dip-dry and annealing, binary cooperative $NiCo_2O_4$ could adhere to the nickel foams robustly with a solution-based surface treatment. The differences in electrochemical tests inspired us to disscuss the process further. From the origin of supercapacitor and nanosized battery materials, the link was established to construct a bridge. The bridged gap highlights some new design ideas as the following: (1) An electrode could combine “supercapacitor” with “battery” rather than two asymmetric electrodes. (2) It may be attractive to design an aqueous high-power battery. (3) It is possible that a pseudocapacitive behavior could be received by binary cooperative battery and double-layer materials.

Acknowledgements

This work was supported by National Natural Science Foundation of China (21353003), Special Innovation Talents of Harbin Science and Technology (2013RFQXJ145), Fundamental Research Funds of the Central University (HEUCFZ), Key Program of the Natural Science Foundation of Heilongjiang Province (ZD201219), Program of International S&T Cooperation special project (2013DFA50480)

Notes

[a] Key Laboratory of Superlight Material and Surface Technology, Ministry of Education, Harbin Engineering University, 150001, PR China.

[b] Key Laboratory of Cluster Science, Mnistry of Education , School of chemistry, Beijing Institute of Technology, 100081, PR China.

[c] State Key Laboratory of Polymer Physics and Chemistry, Changchun Institute of Applied Chemistry, Chinese Academy of Sciences, 130022, PR China.

* Corresponding author: Tel.: +86 451 8253 3026; fax: +86 451 8253 3026; E-mail: junwang@hrbeu.edu.cn.

References

1 S. Z. Butler, S. M. Hollen, L. Cao, Y. Cui, J. A. Gupta, H. R. Gutierrez, T. F. Heinz, S. S. Hong, J. Huang, A. F. Ismach, E. Johnston-Halperin, M. Kuno, V. V. Plashnitsa, R. D. Robinson, R. S. Ruoff, S. Salahuddin, J. Shan, L. Shi, M. G. Spencer, M. Terrones, W. Windl and J. E. Goldberger, *ACS Nano*, 2013, **7**, 2898-2926.
2 R. Ma and T. Sasaki, *Adv. Mater*., 2010, **22**, 5082-5104.
3 M. Osada and T. Sasaki, *Adv. Mater.*, 2012, **24**, 210-228.
4 V. Nicolosi, M. Chhowalla, M. G. Kanatzidis, M. S. Strano and J. N. Coleman, *Science*, 2013, **340**, 1420
5 Y. G. Yao, L. Tolentino, Z. Z. Yang, X. J. Song, W. Zhang, Y. S. Chen and C. P. Wong, *Adv. Funct. Mater.*, 2013, **23**, 3577-3583.
6 C. Nethravathi, B. Viswanath, M. Sebastian and M. Rajamathi, *J. Colloid Interf. Sci.*, 2010, **345**, 109-115.
7 S. Ida, D. Shiga, M. Koinuma and Y. Matsumoto, *J. Am. Chem. Soc.*, 2008, **130**, 14038-14039.
8 J. Zhu, L. Cao, Y. Wu, Y. Gong, Z. Liu, H. E. Hoster, Y. Zhang, S. Zhang, S. Yang, Q. Yan, P. M. Ajayan and R. Vajtai, *Nano Lett.*, 2013, **13**, 5408-5413.
9 J. Feng, X. Sun, C. Wu, L. Peng, C. Lin, S. Hu, J. Yang and Y. Xie, *J. Am. Chem. Soc.*, 2011, **133**, 17832-17838.
10 G. Wang, L. Zhang and J. Zhang, *Chem. Soc. Rev.*, 2012, **41**, 797-828.
11 T. Brezesinski, J. Wang, S. H. Tolbert and B. Dunn, *Nat. Mater.*, 2010, **9**, 146-151.
12 A. S. Arico, P. Bruce, B. Scrosati, J. M. Tarascon and W. van Schalkwijk, *Nat. Mater.*, 2005, **4**, 366-377.
13 X. Dong, L. Wang, D. Wang, C. Li and J. Jin, *Langmuir,* 2012, **28**, 293-298.
14 J. F. Xie, X. Sun, N. Zhang, K. Xu, M. Zhou and Y. Xie, *Nano Energy*, 2013, **2**, 65-74.
15 L. Wang, D. Wang, X. Y. Dong, Z. J. Zhang, X. F. Pei, X. J. Chen, B. Chen and J. Jin, *Chem. Commun.*, 2011, **47**, 3556-3558.
16 X. Lang, A. Hirata, T. Fujita and M. Chen, *Nat. Nanotechnol.*, 2011, **6**, 232-236.
17 L. Jiang, R. Wang, B. Yang, T. J. Li, D. A. Tryk, A. Fujishima, K. Hashimoto and D. B. Zhu, *Pure and Appli. Chem.*, 2000, **72**, 73-81.
18 G. Zhang and X. W. Lou, *Adv. Mater.*, 2013, **25**, 976-979.
19 J. B. Liang, R. Z. Ma, N. B. O. Iyi, Y. Ebina, K. Takada and T. Sasaki, *Chem. Mater.*, 2010, **22**, 371-378.
20 R. Z. Ma, Z. P. Liu, L. Li, N. Iyi and T. Sasaki, *J. Mater. Chem.*, 2006, **16**, 3809-3813.
21 J. Park, J. Joo, S. G. Kwon, Y. Jang and T. *Angew. Chem. Int. Edit.*, 2007, **46**, 4630-4660.
22 H. Colfen and M. Antonietti, *Angew. Chem. Int. Edit*, 2005, **44**, 5576-5591.
23 M. Niederberger and H. Colfen, *Phys. Chem. Chem. Phys.*, 2006, **8**, 3271-3287.
24 M. Duduta, B. Ho, V. C. Wood, P. Limthongkul, V. E. Brunini, W. C. Carter and Y. M. Chiang, *Adv. Energ. Mater.*, 2011, **1**, 511-516.
25 I. E. Rauda, V. Augustyn, B. Dunn and S. H. Tolbert, *Acc. Chem. Res.*, 2013, **46**, 1113-1124.
26 V. Augustyn, J. Come, M. A. Lowe, J. W. Kim, P.L. Taberna, S. H. Tolbert, H. D. Abruña, P. Simon and B. Dunn, *Nat. Mater.*, 2013, **12**, 518-522.
27 B. E. Conway, *J. Electrochem. Soc.*, 1991, **138**, 1539-1548.
28 B. E. Conway, V. Birss and J. Wojtowicz, *J. Power Sources*, 1997, **66**, 1-14.
29 B. E. Conway, *Electrochim. Acta*, 1993, **38**, 1249-1258.
30 B.E.Conway, *New York,* 1999; p 11-32.
31 V. Gupta, S. Gupta and N. Miura, *J. Power Sources*, 2008, **175**, 680-685.
32 V. Gupta, S. Gupta and N. Miura, *J. Power Sources*, 2010, **195**, 3757-3760.
33 X. Wang, X. D. Han, M. Lim, N. Singh, C. L. Gan, M. Jan and P. S. Lee, *J. Phys. Chem. C*, 2012, **116**, 12448-12454.
34 J. B. Goodenough, *Acc. Chem. Res.*, 2013, **46**, 1053-1061.
35 M. Wagemaker and F. M. Mulder, *Acc. Chem. Res.*, 2013, **46**, 1206-1215.
36 W. Dreyer, J. Jamnik, C. Guhlke, R. Huth, J. Moskon and M. Gaberscek, *Nat. Mater.*, 2010, **9**, 448-453.
37 C. Z. Yuan, J. Y. Li, L. R. Hou, X. G. Zhang, L. F. Shen and X. W. Lou, *Adv. Funct. Mater.*, 2012, **22**, 4592-4597.
38 M. Park, X. C. Zhang, M. D. Chung, G. B. Less and A. M. Sastry, *J. Power Sources*, 2010, **195**, 7904-7929.